Using force covariance to derive effective stochastic interactions in dissipative particle dynamics

Anders Eriksson, Martin Nilsson Jacobi, Johan Nyström, and Kolbjørn Tunstrøm
Complex Systems Group, Department of Energy and Environment, Chalmers University of Technology, 41296 Göteborg, Sweden
(Received 12 October 2007; published 16 January 2008)

There exist methods for determining effective conservative interactions in coarse-grained particle-based mesoscopic simulations. The resulting models can be used to capture thermal equilibrium behavior, but the model system we study does not correctly represent transport properties. We suggest the use of force covariance to determine the full functional form of dissipative and stochastic interactions. We show that a combination of the RDF and a force covariance function can be used to determine all interactions in dissipative particle dynamics (DPD). Furthermore, we use the method to test whether the effective interactions in DPD can be adjusted to produce a force covariance consistent with the projection of a microscopic Lennard-Jones simulation. The results indicate that the DPD ansatz may not be consistent with the underlying microscopic dynamics. We discuss how this result relates to theoretical studies reported in the literature.

DOI: 10.1103/PhysRevE.77.016707 PACS number(s): 47.11.−j, 05.40.−a, 45.70.−n, 47.10.−g

I. INTRODUCTION

It is the long-standing aim of molecular simulations to elucidate mechanisms that cannot be directly observed in experiments or understood in terms of more abstract models. Though extremely successful in many areas, when applied to mesoscopic systems, such as membranes or complex fluids, one often finds that the relevant time and length scales on which important mechanisms take place are beyond the reach of direct, detailed simulations. As a consequence, several coarse-grained methods have been developed to allow for a larger time span to be simulated. Lattice gases [1] correspond to dividing the system into an array of subsystems, each a thermodynamic system on its own with a local temperature, pressure, particle density, and velocity distribution. Other coarse-graining procedures have explicit particles with pairwise interactions; well-known examples are united atoms [2], smoothed particle hydrodynamics (SPH) [3], and dissipative particle dynamics (DPD) [4]. There also exist hybrid methods suitable, for example, in molecular simulations where atomistic resolution is needed only in spatially localized domains—e.g., [5,6].

Atomic force fields for molecular dynamics (MD), derived from potentials defined empirically or theoretically (e.g., from quantum-mechanical models), are relatively mature. In contrast, it is much less clear how to choose the effective force fields for coarse-grained models, partly because the connection between the degrees of freedom in the coarse-grained dynamics and the underlying MD differs from one coarse-graining procedure to the next. Frequently, simple heuristic forces are used; partly because of computational ease, but also because the detailed forces may not be known [7]. The magnitude of the forces are then chosen to match the macroscopic observables of the system, such as the compressibility. In [8] (see also references therein), effective forces are calculated for particles interacting according to the Lennard-Jones potential, which corresponds to the average effect of the true forces during a time interval. Because the time-averaged force is effectively an average over rapid fluctuations of close particles, the effective potentials are much softer than the Lennard-Jones potential at small distances. An alternative approach, which we will use later in this paper, is to use the fact that for particle systems with central forces there is a one-to-one relation between the radial distribution of particles at thermal equilibrium and the pairwise potential [9].

When coarse-graining a molecular system, the effective interactions in the resulting system can either be deterministic (smooth, due to averaging of fast degrees of freedom), in which case just matching the equilibrium properties of the system gives the correct dynamics, or the fast degrees of freedom act as a noisy driving force. Which of these two scenarios best describe the system at hand depends on the exchange of energy between the coarse-grained particles and the degrees lost in the coarse-graining procedure. If a substantial amount of energy is exchanged, then the motion of the coarse-grained particles will not be smooth or deterministic. In this case, it is not sufficient to capture the conservative forces, but we must also introduce dissipative and stochastic forces. These forces are included in the SPH and DPD models. The models are quite similar, and in this paper we choose to focus on DPD. As mentioned in the previous paragraph the smooth, or conservative, part of the interaction can be determined from the RDF in thermal equilibrium [9]. In other words, the radial distribution at equilibrium is not affected by the noise term in the interaction (provided an appropriate deterministic dissipative force is added, ensuring the equilibrium temperature). Clearly it follows that equilibrium properties that are determined by the radial distribution are also not affected. Examples are compressibility and other observables defining the equation of state. Other characteristics such as the diffusion coefficient and the viscosity do depend on the stochastic interactions. To capture these properties it is central to choose the stochastic interaction, including its radial dependence, as correctly as possible.

To accurately describe the dissipative and stochastic part of the dynamics we must introduce a new observable, complementing the RDF. A candidate could be the autocorrelation of the velocity, which is directly related to the stochastic driving on a single particle as well as the diffusion coefficient through Green-Kubo relations [10,11]. In a particle-based mesoscopic model such as DPD, the stochastic interaction is represented as a force between the particles.

Clearly this interaction must have a radial dependence (typically with short range). A useful observable for estimating the stochastic interaction must therefore be able to resolve the radial dependence. In this paper we suggest the use of the force covariance function as a candidate for such an observable and use DPD as a test case for the method.

II. DISSIPATIVE PARTICLE DYNAMICS

DPD was introduced in 1992 by [4] as a simulation technique for hydrodynamic phenomena. The method has received much theoretical attention [12–16], which provides support for this kind of model and has been established as a standard method for mesoscopic simulation. Among other things DPD has been used to study complex fluids [7], spontaneous self-assembly of amphiphilic molecules into bilayered membranes [17], vesicles [18,19], and hydrodynamics [20]. In its standard form, DPD is a particle model with pairwise interactions, quite similar to MD, but with a dissipative and stochastic contribution to the interactions between the particles.

In its simplest form, the equations of motion for a DPD model, with mesoscopic particles positioned at $\mathbf{r}_i$, and with velocities $\mathbf{v}_i$ and momenta $\mathbf{p}_i$, can be written as a system of Langevin equations

$$\dot{\mathbf{r}}_i = \mathbf{v}_i,$$

$$\dot{\mathbf{p}}_i = \sum_{j \neq i} [\mathbf{F}_{ij}^{\mathrm{C}} + \mathbf{F}_{ij}^{\mathrm{D}} + \mathbf{F}_{ij}^{\mathrm{S}}], \tag{1}$$

where $\mathbf{F}_{ij}^{\mathrm{C}}$, $\mathbf{F}_{ij}^{\mathrm{D}}$, and $\mathbf{F}_{ij}^{\mathrm{S}}$ are the conservative, dissipative, and stochastic forces between particles i and j. Both the conservative and nonconservative interactions in DPD are modeled by central forces obeying Newton's third law, ensuring that (angular) momentum is conserved [4]. The dissipative and stochastic forces are

$$\mathbf{F}_{ij}^{\mathrm{D}} = -\omega^{D}(r_{ij})\mathbf{e}_{ij} \cdot (\mathbf{v}_i - \mathbf{v}_j)\mathbf{e}_{ij}, \tag{2}$$

$$\mathbf{F}_{ij}^{\mathrm{S}} = \omega^{S}(r_{ij})\zeta_{ij}\mathbf{e}_{ij}, \tag{3}$$

where r_{ij} is the distance between particles i and j, and $\mathbf{e}_{ij}$ is the unit vector pointing from j to i. The scalar functions $\omega^{\mathrm{D}}(r_{ij})$ and $\omega^{\mathrm{S}}(r_{ij})$ describe friction and noise, respectively. ζ_{ij} is interpreted as a symmetric Gaussian white noise term with mean zero and covariance,

$$\langle \zeta_{ij}(t)\zeta_{i'j'}(t') \rangle = (\delta_{ii'}\delta_{jj'} + \delta_{ij'}\delta_{ji'})\delta(t - t'), \tag{4}$$

where δ_{ij} and $\delta(t)$ are the Kronecker and Dirac delta functions. Assuming that the equilibrium distribution of a DPD system is given by the canonical ensemble, the fluctuation-dissipation theorem leads to a relation between the dissipative and stochastic parts [12]:

$$\omega^{\mathrm{D}}(r) = (2k_B T)^{-1}[\omega^{\mathrm{S}}(r)]^2. \tag{5}$$

For simplicity, we drop the superscript and write $\omega(r) \equiv \omega^{\mathrm{S}}(r)$. Equations (1)–(5) together establish the general form of the DPD dynamics. Both the conservative force $\mathbf{F}_{ij}^{\mathrm{C}}$, or equivalently the corresponding scalar potential, and the scalar function $\omega(r)$ depend on the particular system of interest and need to be determined to obtain the correct DPD model. In practice, this is the difficult part of DPD and also the rationale behind the heuristic approach in deciding the interactions. As an example, the common practice for fluid-like systems is to apply linear functions with a cutoff radius r_c:

$$\mathbf{F}_{ij}^{\mathrm{C}} = (1 - r_{ij}/r_c)a_{ij}\chi_{ij}\mathbf{e}_{ij} = F^{\mathrm{C}}(r_{ij})\mathbf{e}_{ij}, \tag{6}$$

$$\omega(r_{ij}) = (1 - r_{ij}/r_c)\sigma\chi_{ij}, \tag{7}$$

where a_{ij} is the strength of the conservative force between particles i and j, σ is the amplitude of the noise, and χ_{ij} is 1 for $r_{ij} \leq r_c$ and 0 elsewhere.

Despite its popularity and theoretical support, it is unclear how DPD should be interpreted as a coarse-grained model [21]. One point of view, and the one we will elaborate on in this paper, is to consider DPD as a systematic coarse-graining of an underlying atomistic system. If the DPD method could be shown to have a firm microscopic foundation, that would greatly impact our ability to couple DPD to actual physical systems. Several authors—e.g., [22–25]—have established bottom-up connections between the microscale and mesoscale and obtained mesoscopic dynamics resembling DPD. The resulting methods differ from DPD as they incorporate the geometry of the system in the equations, implying forces that are not central or pairwise, while DPD is a model with only pairwise interactions. It is clear that the validity of DPD as a coarse-grained model, or how well DPD represents an underlying microscopic system, has not been fully resolved.

To obtain a well-defined bottom-up scheme, the dynamics of the coarse-grained DPD particles must be defined through a projection of the microscopic trajectories. The problem is to find a closed representation of the system at the coarse-grained level—i.e., to determine all interactions in the DPD model. In this paper we investigate a method of estimating the DPD interactions using measurements on the coarse-grained level of a simulation. By applying the method to a typically assumed projection of a microscopic system, we clarify some important aspects of DPD as a systematically coarse-grained model.

The DPD technique has its theoretical foundations in Mori-Zwanzig theory on projection operators [26–29]. In short, the theory states that given a microscale dynamics, a lower-dimensional representation can be formally attained through a projection of the phase space, where fast degrees of freedom are treated as Markovian (white) noise [26]. This framework can be applied to MD [30,31]. Naturally, how faithfully the coarse-grained model will represent the underlying dynamics depends on the choice of projection. The DPD method assumes a projection resulting in a mesoscopic model characterized as a particle-based Langevin dynamics with pairwise and negated central forces. The internal degrees of freedom in the mesoscopic particles give rise to dissipation and noise, which is captured by nonconservative

pairwise interactions. As a consequence, sufficiently close to equilibrium, one obtains the classical result of the asymptotic $t^{-d/2}$ decay of the velocity autocorrelation (d is the dimensionality of the system) [32]. In addition, the interactions give rise to hydrodynamic modes in the fluid [32,33], which lead to the Navier-Stokes equations on the macroscopic level [34].

III. ESTIMATING THE EFFECTIVE FORCES

Given the DPD ansatz for the effective equations of motion, the question is, how does one find the conservative and dissipative forces $F^C(r)$ and $\omega(r)$? In this section we present the theoretical motivations for our method and apply it to DPD simulations to test the accuracy of the method on a case where we know the ansatz to be true. In Sec. IV we apply the method to a coarse-graining of a system of particles interacting via the Lennard-Jones potential in order to see how the method fares on a classical MD system.

A. Conservative force term

The original motivation [7] for a repulsive conservative force was a measurement of the effective potential for the interaction between particles in a Lennard-Jones fluid [8]. More generally applicable methods for estimating the conservative interactions are based on the radial distribution function (RDF) in thermal equilibrium [35–40]. In these reports, the estimate of the conservative force is obtained using a result by [9], stating that the difference between two pairwise potentials that give rise to the same RDF must be a constant gauge shift, and hence of no physical significance. The importance of this theorem lies in the one-to-one correspondence between potential and RDF.

The conservative interactions are determined by the RDF alone, which in turn is determined by the thermal equilibrium of the system. As long as the fluctuation-dissipation theorem holds, the thermal equilibrium is independent of the specific form of the dissipative and random interactions [12], and it follows that we can estimate the conservative forces from a given RDF independently of the stochastic forces. Here we use the inverse Monte Carlo method of Lyubartsev and Laaksonen [41], which starts from a Boltzmann ansatz of the potential and then, through iteration, finds a potential giving rise to the desired RDF. In what follows we briefly describe the method, following [41].

The connection between the RDF and the potential can be found from the Hamiltonian of the system. Consider a system of particles with pairwise interactions. It can be discretized as

$$H = \sum_{\alpha} \Phi_{\alpha} S_{\alpha}, \tag{8}$$

which corresponds to using a stepwise constant potential Φ_{α}. S_{α} denotes the number of particle pairs separated by a distance in the range from r_{α} to $r_{\alpha+1}$, where $r_0=0$, $r_1=dr$, and $r_{\alpha}=\alpha \cdot dr$. The average of S_{α} is directly connected to the RDF $g(r)$ by the relation

$$\frac{\langle S_{\alpha} \rangle}{N(N-1)/2} = \frac{V_{\alpha}}{L^3} g(r), \tag{9}$$

where N is the number of particles, L^3 the volume of the simulation box, and V_{α} the volume of the spherical shell between radii r_{α} and $r_{\alpha+1}$. Using a Monte Carlo (MC) approach, the system may be simulated with a start potential $\Phi_{\alpha}^{(0)}$. It is common practice to choose this to be the potential of mean force,

$$\Phi_{\alpha}^{(0)} = -k_B T \ln g(r_{\alpha}). \tag{10}$$

The correspondence between potential and RDF is an equilibrium result and hence only valid for fixed temperatures and densities. These quantities must therefore be the same in the MC simulation as they were in the original simulation from which the RDF was obtained.

Simulating with the trial potential $\Phi_{\alpha}^{(0)}$ produces an $\langle S_{\alpha}^{(0)} \rangle$ which may differ from the correct value S_{α}^{*}. The difference $\Delta \langle S_{\alpha} \rangle^{(0)} = \langle S_{\alpha} \rangle^{(0)} - S_{\alpha}^{*}$ is used to find a new trial potential by solving for $\Delta\Phi$ in the linear equation system,

$$\Delta \langle S_{\alpha} \rangle = \sum_{\gamma} \frac{\partial \langle S_{\alpha} \rangle}{\partial \Phi_{\gamma}} \Delta \Phi_{\gamma}, \tag{11}$$

with $\frac{\partial \langle S_{\alpha} \rangle}{\partial \Phi_{\gamma}}$ given by [41]

$$\frac{\partial \langle S_{\alpha} \rangle}{\partial \Phi_{\gamma}} = -\frac{\langle S_{\alpha} S_{\gamma} \rangle - \langle S_{\alpha} \rangle \langle S_{\gamma} \rangle}{k_B T}. \tag{12}$$

The next guess for potential is then $\Phi^{(1)}=\Phi^{(0)}-\Delta\Phi$. This procedure is repeated until Φ has converged to a potential that reproduces the original RDF.

The potential of the mean force is usually a good first approximation to the final potential, and convergence to a unique potential normally takes less than ten updates in the Monte Carlo simulations. This is especially true for the soft coarse-grained potentials we get from considering effective interactions between clusters of particles. For instances that nevertheless require special care, problems with convergence for the potential over successive MC simulations can generally be overcome by moving only a fraction in the direction specified by Eq. (11).

B. Dissipative force term

Assuming that the DPD ansatz is valid, the functional form of the dissipative term [and through the fluctuation dissipation theorem, Eq. (5), the stochastic term] can be isolated through a Kramer-Moyal expansion [42] of Eq. (1):

$$-\langle \delta\mathbf{p}_i \cdot \delta\mathbf{p}_j\rangle/\delta t = \langle \omega^2(r_{ij})\rangle - \sum_{k\neq i,l\neq j} \langle \mathbf{F}^{\mathrm{C}}_{ik} \cdot \mathbf{F}^{\mathrm{C}}_{jl}\rangle \delta t - \sum_{k\neq i,l\neq j} \frac{\langle \omega^2(r_{ik})\omega^2(r_{jl})(\mathbf{e}_{ik}\cdot\mathbf{v}_{ik})(\mathbf{e}_{jl}\cdot\mathbf{v}_{jl})(\mathbf{e}_{ik}\cdot\mathbf{e}_{jl})\rangle}{(2k_BT)^2}\delta t$$
$$+ \sum_{k\neq i,l\neq j} \frac{\langle \omega^2(r_{ik})(\mathbf{e}_{ik}\cdot\mathbf{v}_{ik})(\mathbf{e}_{ik}\cdot\mathbf{F}^{\mathrm{C}}_{jl})\rangle}{2k_BT}\delta t + \sum_{k\neq i,l\neq j} \frac{\langle \omega^2(r_{jl})(\mathbf{e}_{jl}\cdot\mathbf{v}_{jl})(\mathbf{e}_{jl}\cdot\mathbf{F}^{\mathrm{C}}_{ik})\rangle}{2k_BT}\delta t + O(\delta t^2), \tag{13}$$

where $\delta\mathbf{p}_i(t)=\mathbf{p}_i(t+\delta t)-\mathbf{p}_i(t)$. All averages in Eq. (13) have the condition that the distance r_{ij} between particles i and j must equal r. This equation provides a relationship between the functional form of the stochastic and dissipative interactions, $\omega(r)$, and the force covariance κ_{F} defined as

$$\kappa_{\mathrm{F}} \equiv -\langle \delta\mathbf{p}_i \cdot \delta\mathbf{p}_j\rangle/\delta t. \tag{14}$$

In the DPD simulations we can take δt small enough that only the leading term of Eq. (13) is significant. If the microscopic dynamics is deterministic, as in most MD, there generally exists a time scale below which the forces are smooth functions of time (this is the time scale on which the MD can be integrated). On this time scale, the projected dynamics is also smooth (if the projection is smooth), but not autonomous. It follows that for small δt the force covariance κ_{F} is proportional to δt, corresponding to $\omega(r)=0$ in Eq. (13).

In fluids, the magnitude of κ_{F} will typically increase with increasing δt, because on relatively short time scales the particles of the fluids oscillate in a cage formed by their closest neighbors (the Franck-Rabinowitch effect). We consider these rapid fluctuations to correspond to fast degrees of freedom in the system. To get an idea of the time scales involved, consider water particles in a fluid at normal pressure and room temperature. The particles' distance to their closest neighbors oscillates around the first peak in the RDF at approximately 0.28 nm. The half-width of the peak, approximately 0.05 nm, gives an indication of how far the molecule travels before experiencing strong repulsive forces from other particles. We estimate the typical velocity as the root-mean-square (rms) velocity

$$v_{\mathrm{rms}} = \sqrt{\langle \mathbf{v}^2\rangle} = \sqrt{3k_{\mathrm{B}}T/m}. \tag{15}$$

At room temperature (25°C), the rms velocity is approximately 640 m/s. One may argue that the orientations of the particle velocities are essentially random, so that the rms difference in velocity is $v_{\mathrm{rms}}\sqrt{2}$ and that they collide at half the half-width. The time to travel this distance at the typical velocity is then approximately 0.03 ps, and we take this as a rough approximation to the time scale at which the fast dynamics occur. It is only at time scales significantly larger than this time scale that we can expect to approximate the fast degrees of freedom with a spatially structured but Markovian noise as in the DPD ansatz. On this time scale, the fluid approaches a local thermal equilibrium on the length scale of the coarse-grained particles, determined by the local concentration, local average velocity, and kinetic energy [32].

As a consequence, it is generally not possible to take the limit of $\delta t \to 0$ in the numerically estimated κ_{F} to find $\omega(r)$. Rather, we will assume that there exists a time interval where the fast degrees of freedom can be approximated by noise and where κ_{F} is an approximately linear function of time. Given two values of δt in this interval, δt_1 and δt_2, we can use Richardson extrapolation to eliminate the δt term in Eq. (13) to obtain an $O(\delta t^2)$ estimate for $\omega^2(r)$:

$$\omega^2(r_{ij})|_{\delta t_0} \approx \frac{\delta t_1}{\delta t_2}\frac{\langle \delta\mathbf{p}_i\cdot\delta\mathbf{p}_j\rangle|_{\delta t_2}}{\delta t_2-\delta t_1} - \frac{\delta t_2}{\delta t_1}\frac{\langle \delta\mathbf{p}_i\cdot\delta\mathbf{p}_j\rangle|_{\delta t_1}}{\delta t_2-\delta t_1}. \tag{16}$$

An alternative approach is to do a linear fit with respect to δt in this region, for each value of r, and from the best fit take the intersection with the line $\delta t=0$.

C. Recreating the effective interactions of DPD simulations

At this point we have established the principles behind our method. An important consistency check is to apply the method to standard DPD simulations, where the dynamics is truly Langevinian. This was done by performing DPD simulations with different functional forms of both $\mathbf{F}^{\mathrm{C}}_{ij}(r)$ and $\omega(r)$. Using standard DPD units, the simulation region was a periodic cubic box with side length $L=8.7359$, with 3 particles per volume unit, giving a total of 2000 particles. From the simulations, the RDF and κ_{F} were calculated for 100 r values in the range 0–1.75, after which the RDF had converged to 1.0. The time-step size used in the simulations was

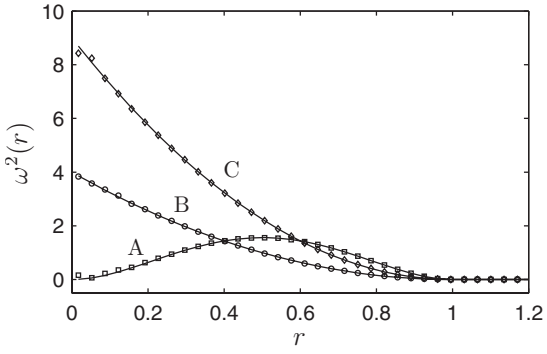

FIG. 1. The plots show three different functional forms of $\omega^2(r)$. The symbols ◇, ◯, and □ show the values found by our method: measuring κ_{F} of a DPD simulation. The exact functional forms used in the simulations are plotted as solid lines. All units are standard DPD units. The conservative and dissipative forces are (for $r\in[0,1]$): (a) $F^{\mathrm{C}}(r)=10(1-r)$, $\omega(r)=5r(1-r)$, (b) $F^{\mathrm{C}}(r)=10(1-r)$, $\omega(r)=2(1-r)$, and (c) $F^{\mathrm{C}}(r)=10r(1-r)$, $\omega(r)=3(1-r)$. For $r>1$, both functional forms are zero.

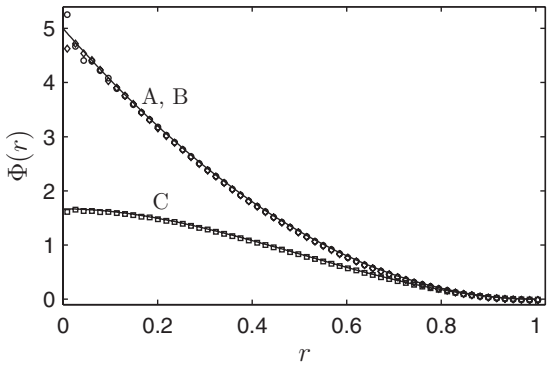

FIG. 2. The conservative potentials $\Phi(r) \equiv \int_r^\infty dr' F^C(r')$ from three DPD simulations have been recreated from RDF data. Cases (a) and (b) correspond to a linear DPD-force (i.e., quadratic potential) with different random force parts. For case (c), a quadratic conservative force was used. For details, see caption of Fig. 1. In all three cases, the potential was exactly recreated up to statistical accuracy.

small ($\delta t = 10^{-3}$) compared to a normal DPD simulation. The reason for this was to approach the limit of small δt, so that the terms proportional to δt could be ignored in Eq. (13); $\omega^2(r)$ is then given simply by κ_F.

In all cases the method accurately recreated the DPD interactions used in the simulations. Figure 1 shows the results of recreating $\omega^2(r)$ for three different functional forms. The conservative potential was also varied (see figure caption for details), and plots of recreated potentials from these simulations are shown in Fig. 2.

An example of the situation where we cannot measure κ_F in the limit $\delta t \to 0$ is shown in Fig. 3. Here two measurements of κ_F from a DPD simulation using time steps of different sizes ($\delta t_1 = 0.025$ and $\delta t_2 = 0.05$) deviate clearly from $\omega^2(r)$. The resulting estimate of $\omega^2(r)$, obtained by Richardson extrapolation of κ_F measurements, falls close on the original curve. It should be noted that κ_F measurements are obtained from the same simulation (with time step $\delta t = 0.005$), as an increase in the DPD time step would alter the

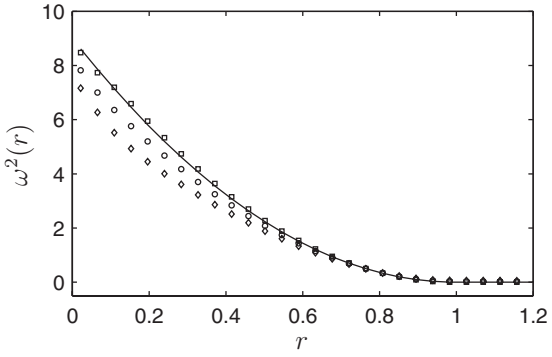

FIG. 3. The plot shows two measurements of κ_F obtained from a DPD simulation using time steps of different size [$\delta t_1 = 0.025$ (◯) and $\delta t_2 = 0.05$ (◇)]. The resulting estimate of $\omega^2(r)$, obtained by Richardson extrapolation of κ_F measurements, is shown as open squares (□). The solid line shows the exact form of $\omega^2(r) = [3(1-r)]^2$ used in the simulation. The conservative force used was $F^C(r) = 10r(1-r)$.

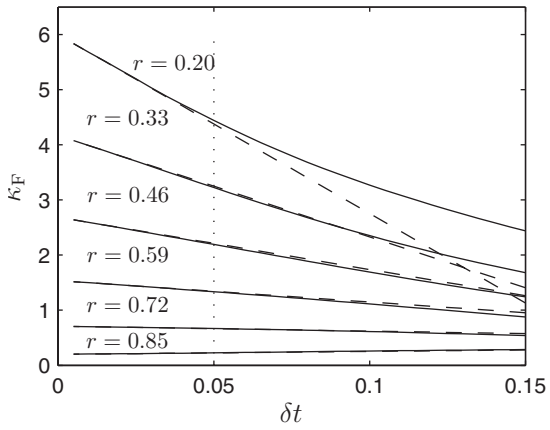

FIG. 4. The force covariance κ_F measured in DPD simulation plotted as a function of δt for different values of r (solid lines). The simulation setup is the same as in Fig. 3. It is clearly visible that κ_F has a linear region for small δt (marked by dotted vertical line), as expected from Eq. (13). The dashed lines are linear functions with slopes given by the derivatives of κ_F close to $\delta t = 0$.

dynamics of the system. For a projected dynamics this is not a problem, as it evolves on the microscopic time scale. In Fig. 4 measurements of κ_F from the same simulation are plotted against the size of the time difference between measurements, δt. As predicted by Eq. (13) the system exhibits a linear behavior for small values of δt (in this case $\delta t \lesssim 0.05$). Note, however, that how far the linear region extends varies significantly with the value of r.

IV. COARSE-GRAINING OF A LENNARD-JONES FLUID

We now apply the method to a coarse-grained molecular system. Because of its simple form and because it is so well understood, we examine the case of a coarse-grained two-dimensional Lennard-Jones (LJ) fluid. This is a single-species fluid, where the particles interact according to the standard pairwise potential

$$V(r) = 4\epsilon[(r/\sigma_{LJ})^{-12} - (r/\sigma_{LJ})^{-6}]. \tag{17}$$

The parameters are chosen to correspond to bulk water at room pressure and temperature: the energy $\epsilon = 6.739$ meV, the interaction length $\sigma_{LJ} = 0.31655$ nm, and the mass $m_{LJ} = 2.99 \times 10^{-26}$ kg.

In DPD, the particles are often understood to be a collection of underlying particles, with properties such as mass and momentum defined from these. According to this view, we follow [22], where the coarse-grained dynamics is expressed in terms of a set of N mesoscopic particles. Each particle has a position $\mathbf{R}_k$, a velocity $\mathbf{U}_k$, and a mass M_k. The instantaneous momentum of mesoscopic particle k is defined as the sum of the momenta of the microscopic particles for which k is the nearest mesoscopic particle, and the mass of the particle is defined as the total mass of these underlying particles:

$$M_k = \sum_{i=1}^{n} \xi_k(\mathbf{r}_i) m_i,$$

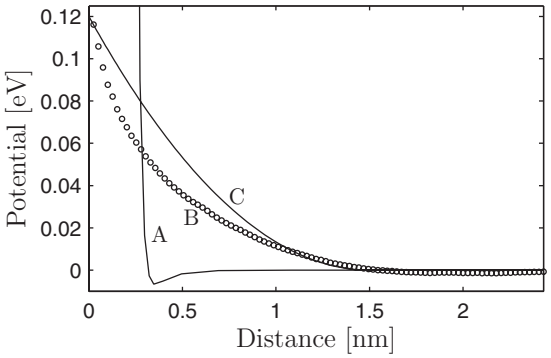

FIG. 5. (A) Lennard-Jones potential used to simulate the microscopic particles. (B) The effective potential for the coarse-grained system, obtained using the inverse MC method. (C) The standard quadratic DPD potential, scaled to the same magnitude as the estimated potential. The main characteristics of DPD—soft-core repulsion and finite support—are confirmed by the retrieved potential.

$$\mathbf{P}_k = \sum_{i=1}^{n} \xi_k(\mathbf{r}_i) m_i \mathbf{v}_i,$$

$$\mathbf{U}_k = \dot{\mathbf{R}}_k = \mathbf{P}_k / M_k. \tag{18}$$

Here n is the total number of microscopic particles, and m_i, $\mathbf{r}_i$, and $\mathbf{v}_i$ represent masses, positions, and velocities, respectively, of the microscopic particles. $\xi_k(\mathbf{r}_i)$ is 1 if mesoscopic particle k is closer to microscopic particle i than any other mesoscopic particle is and 0 otherwise.

Though we use Eqs. (18) to find the motion of the mesoscopic particles, it is nevertheless illuminating to see how the effective forces acting on the mesoscopic particles are related to the forces acting on the microscopic particles. Formally, we calculate the time derivative of the momentum of the mesoscopic particle k in Eq. (18). Between each passage of a microscopic particle from one mesoscopic particle to the next, $\xi_k(\mathbf{r}_i)$ is constant (either 0 or 1). During these time intervals, the effective force acting on the mesoscopic particle is the sum of the forces acting on the microscopic particles closest to k:

$$M_k \dot{\mathbf{U}}_k = \sum_{i=1}^{n} \xi_k(\mathbf{r}_i) \mathbf{f}_i. \tag{19}$$

Suppose microscopic particle i leaves mesoscopic particle k. When this happens, the mesoscopic particle experiences an impulse

$$\mathbf{I} = \Delta M_k \mathbf{U}_k = -m_i \mathbf{v}_i, \tag{20}$$

so that the velocity of mesoscopic particle k changes instantaneously from $\mathbf{U}_k$ to

$$\mathbf{U}_k' = \frac{1}{M_k - m_i}(M_k \mathbf{U}_k - m_i \mathbf{v}_i). \tag{21}$$

The receiving mesoscopic particle is subject to the opposite impulse $-\mathbf{I}$ (formally, it is possible to express the force in terms of Dirac's δ function).

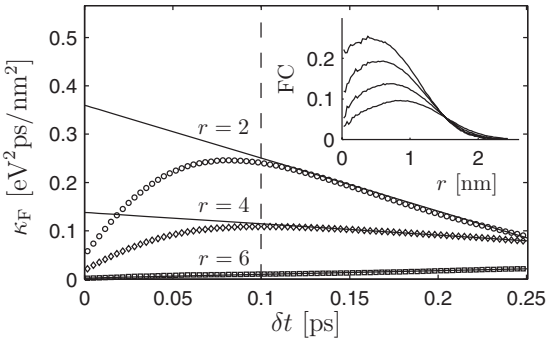

FIG. 6. The force covariance κ_F as a function of δt (symbols) for three values of r (shown by each curve). κ_F is approximately linear for large enough δt (to the right of the dashed line). For each value of r, the extrapolation of this region (indicated by solid lines) to δt=0 determines the values of $\omega^2(r)$; cf. Eq. (13). Inset: κ_F as a function of r for δt=0.1 ps (top) and 0.15 ps, 0.2 ps, and 0.25 ps (bottom). It is clear from this figure that the terms proportional to δt are not negligible in Eq. (13).

Finally, a word of caution: It might seem natural to use Eq. (19) alone to define the motion of the mesoscopic particles; however, in this dynamics the total momentum in the mesoscopic system changes when a microscopic particle moves from one mesoscopic particle to another.

A. Estimated forces

The conservative interaction was determined from the RDF of the mesoscopic particles by the inverse MC method discussed earlier. The RDF was measured in LJ simulations with 1600 particles in a simulation box with side length 12.48 nm, temperature 333 K, and periodic boundaries. In the coarse-grained description, 160 particles were used, resulting in an average of 10 microscopic particles per mesoscopic particle. Figure 5 shows the potential compared with both the LJ potential (17) and the standard DPD potential (6). The retrieved potential confirms the main characteristics

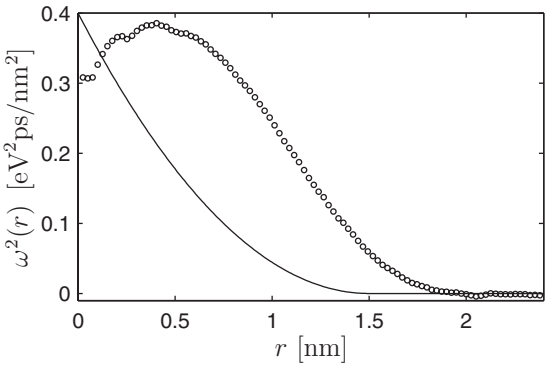

FIG. 7. The plotted circles show the estimate of $\omega^2(r)$, calculated from the force covariance κ_F using Richardson extrapolation; cf. Fig. 6. The solid line is $\omega^2(r)$, using the DPD form in Eq. (7), with the same cutoff distance as for the conservative potential in Fig. 5. The estimated stochastic interaction differs significantly from the function commonly used in DPD studies.

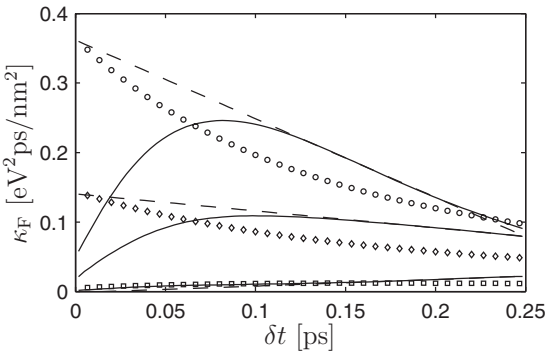

FIG. 8. The plot shows measurements of the force covariance κ_F plotted as a function of δt for both the LJ projection (solid lines) and a DPD simulation (symbols) using the estimated functional forms. Also plotted is the Richardson extrapolation of the LJ projection (dashed lines). The curves are plotted for three values of r (same as in Fig. 6). The linear region of κ_F for the DPD dynamics lies between $\delta t=0$ and $\delta t=0.05$ ps, while the linear region of the projected dynamics is in the range from $\delta t=0.1$ to $\delta t=0.25$ ps. κ_F for the two systems do not have a coinciding linear region (for each value of r).

of the standard DPD potential—i.e., soft-core repulsion and finite support.

In Fig. 6 we show κ_F for the Lennard-Jones system as a function of δt for different values of r (the inset shows κ_F as a function of r for different values of δt). For small δt, κ_F is increasing up to a maximum. We find a range starting at $\delta t=0.1$ ps where κ_F is approximately linear. In principle, κ_F is also linear for very small values of δt, but since we know that the fluctuations we want to approximate with Markovian noise occurs on time scales $\lesssim 0.03$ ps (cf. Sec. III B), we reject this region. Hence, the linear region in the figure should match the linear region of Eq. (13). An extrapolation using data from the linear region gives the shape of $\omega^2(r)$ shown in Fig. 7. For comparison we have also included the standard shape of $\omega^2(r)$, which can be derived from Eq. (7), with the magnitude scaled to fit the obtained $\omega^2(r)$ (solid line). We note that the dissipative force derived from the mesoscopic particle motion is significantly broader than the standard shape. The conservative force is increasing only gradually as a pair of mesoscopic particles come within the interaction distance (approximately 1.5 nm); the dissipative force grows much more rapidly.

B. Consistency check

To test if the projected LJ system can be represented by pairwise Langevinian dynamics, we perform a DPD simulation using the estimated functional forms of the conservative and dissipative forces, as shown in Figs. 5 and 7. Setting up the DPD simulation so as to correspond to the projected LJ dynamics, we obtained measurements of κ_F for varying δt. In Fig. 8 the results (symbols) for a selection of r values are plotted together with the corresponding measurements from the LJ projection (solid lines) and the Richardson extrapolation of these (dashed lines). The linear region of κ_F for the DPD dynamics lies between $\delta t=0$ and $\delta t\approx 0.05$ ps. As pointed out in Sec. III B, this is in the region of the fast dynamics for the underlying system. Clearly, the linear regions for κ_F in the DPD system and in the projected Lennard-Jones system do not coincide and therefore we cannot confirm that the projection can be formulated in terms of DPD.

As is seen in Sec. III B, the method we have developed works for any system that obeys the DPD ansatz. More strictly, it works for any system that evolves on a time scale where all terms of order $O(\delta t^2)$ can be neglected in Eq. (13). That allows $\omega(r)$ to be estimated either directly from κ_F (if also first-order terms of δt are negligible) or through Richardson extrapolation of κ_F for different values of δt. If we only have data available for the system on a longer time scale, there may not be a region where κ_F is approximately linear. In this case it is not possible to use the linearization procedure to extract the dissipative force.

An important remark is that, in general, it cannot be concluded from measurements of κ_F alone if the dynamics is Markovian or follows the DPD ansatz; a cross-check with a DPD simulation is necessary. In the case of the projected LJ dynamics, it was reasonable to assume that the linear region (see Fig. 6) could be interpreted as the right time scale to consider for extracting the functional forms. However, κ_F from the DPD simulation turned out to have its linear region on a much shorter time scale than assumed for the projected dynamics.

In the light of this result, there are two explanations for the observed deviations from the DPD ansatz, which differ with respect to whether the DPD ansatz is correct or not. If we first assume that the projected system follows the DPD ansatz, our guess of a linear region is not correct, and it follows that higher-order terms of δt will affect the value of κ_F, rendering our method inapplicable for this case. The solution to this problem calls for more sophisticated methods to estimate $\omega(r)$ from κ_F. The second possibility is that the projection does not produce a dynamics that follows the DPD ansatz. This could either simply be a result of our choice of projection, or it could point to deeper problems with constructing a coarse-graining scheme that leads to the DPD model.

Flekkøy and co-workers [22–24] have used the same type of projection as presented in this paper [cf. Eq. (18)], but rather than considering the coarse-grained entities as spherical particles, they consider them as cells on a Voronoi lattice. Within each cell, the fluid is assumed to correspond to an ideal fluid at a given pressure, temperature, and velocity. Because of this, the system is similar in spirit to the Lattice-Boltzmann coarse-graining, but with dynamic cells. An advantage of this method is that the dissipative part of the evolution equations can be derived theoretically [24]. However, this method involves keeping track of, and updating, the Voronoi lattice at each time step of the simulation, rendering this technique much slower than standard DPD. As the construction of the Voronoi lattice depends explicitly on all particle positions in the simulation, it also introduces a need for higher-order interactions than the simple pairwise central forces normally associated with DPD. If it proves impossible to find a projection giving rise to DPD dynamics on the coarse-grained level (which is a question that calls for

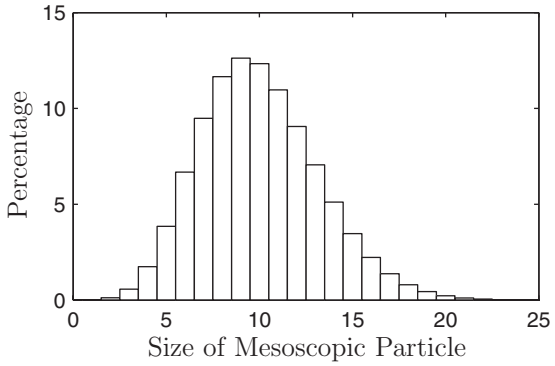

FIG. 9. Size distribution of mesoscopic particle masses, measured in units of microscopic particle masses. The data were obtained from a simulation using 1600 microscopic and 160 mesoscopic particles, giving an average mesoscopic particle size of 10.

further investigation), this alternative approach might still provide a reasonable path to take for performing reliable mesoscopic simulations.

V. CHOICE OF PROJECTION

Although the projection used in this study, Eqs. (18), seems like a natural choice for DPD, it is a problem that the positions of the coarse-grained particles only weakly reflect the positions of the underlying particles. As is shown in Fig. 9, the number of microscopic particles per coarse-grained particle (i.e., the mass of the coarse-grained particle) exhibits large fluctuations, in sharp contrast to the standard DPD model where the masses of all particles are assumed to be equal and constant in time.

One way to make the coarse-grained particles more closely reflect the density variations in the underlying system

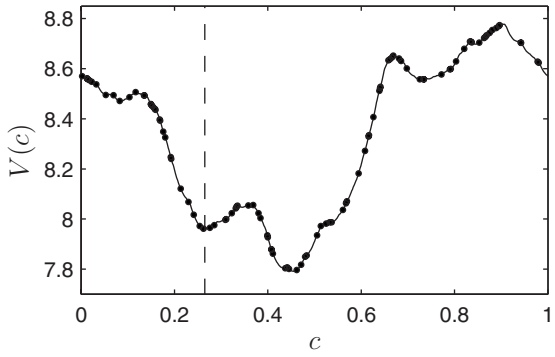

FIG. 10. The figure illustrates how the *k*-means clustering algorithm works. A minimum in the potential landscape corresponding to a local minimum in the sum of squares function (22) is found (indicated by vertical line). The small dots represent particle positions x_i in Eq. (22), and $V(c)$ is the sum-of-squares distance as a function of cluster center position. This example is made for illustrative purposes and therefore contains only a single cluster center to which all the particles belong. As the particles move, $V(c)$ changes, with the effect that local minima are continuously created and destroyed. This process results in discontinuous trajectories for the cluster center positions.

of microscopic particles is to change the projection to incorporate movement of coarse-grained particles toward regions of higher particle concentrations. This can be achieved by using, for instance, the standard *k*-means clustering method [43] (or any other position-based clustering algorithm) to calculate the positions of the coarse-grained particles given the positions of the underlying particles. This results in a model where the coarse-grained particles can be seen as clusters of underlying particles, with each cluster center representing a local concentration peak of microscopic particles. An implementation has been made using this projection, and the results reveal some new difficulties not easily foreseen in advance. With this type of projection, the cluster centers move in a potential landscape of the kind depicted in Fig. 10 for a one-dimensional system, where each local minimum of the curve represents a possible cluster center position. The simulation was made for illustrative purposes, with a single cluster center in a one-dimensional box with $N=100$ particles and with periodic boundary conditions. The curve represents the sum-of-squares distance from all the particles to the cluster center—i.e.,

$$V = \sum_{i=1}^{N} \min(|c - x_i|^2, |L - c + x_i|^2), \tag{22}$$

where the minimum of the distance between the cluster and all periodically displaced images of particle i is used.

By differentiating Eq. (22) with respect to the cluster center position c, it is easily shown that a minimum in the sum-of-squares function represents a local average of the positions of the microscopic particles belonging to the cluster. This information is just what the *k*-mean clustering algorithm uses to calculate the cluster center positions. The fact that the example in Fig. 10 contains only one cluster to which all the particles belong does not change the qualitative outcome that several local minima exist in the potential landscape. The result of this is inevitably that the cluster center positions, represented by a given minimum in the potential landscape, will move with that local minimum until it disappears, which happens frequently in the course of the simulation—for instance, by the merging of two originally separated minima. At this point, the cluster center will jump to the adjacent minima, and in doing so it affects the neighboring cluster centers, resulting in discontinuous movement of the coarse-grained particles. As discontinuous particle movement on the coarse-grained level, due only to strictly local interactions on the microscopic level, is highly unsatisfactory, this type of position-based projections also leave much to be desired.

VI. SUMMARY

In this paper we have developed a method for estimating the forces between particles in a system that evolves according to the DPD ansatz—i.e., Langevinian dynamics with pairwise central forces. The method works well for estimating both conservative and dissipative forces (with the stochastic force given by the dissipative through a fluctuation-dissipation theorem) and should work on any system that follows the DPD ansatz, as long as the time scale is small

enough to let $\omega(r)$ be estimated from the force covariance κ_F. When applied to a projected dynamics of a Lennard-Jones system, we cannot conclude that the projection results in a DPD-like dynamics. The result points toward two possibilities: Either the projected dynamics is DPD-like, but outside the reach of our method, or in the worst case, there might be problems considering DPD as the result of a systematic coarse-graining method.

A natural extension of the work presented in this paper is to examine systems where artifacts due to fluctuating mass and identity problems are not encountered, such as the frequently used united-atoms approach. A simple example would be to coarse-grain water by letting the coarse-grained particle be the whole water molecule. Some work in this direction has already been made by [44]. Another direction is to develop a more sophisticated method for estimating $\omega(r)$ from κ_F.

As we suspect that the linear ansatz for κ_F is too simple, one might be tempted to simply use polynomials of higher degree in δt and do a regression for the coefficient for each value of r separately, based on the region where we think the DPD theory is valid. Since κ_F is close to linear in this region, however, the result of extrapolating the resulting function to find the intersection with the $\delta t=0$ axis may be rather sensitive to the precise choice of region in δt and to noise in the measurement of κ_F (from the finite number of samples).

Rather, one may consider going in the other direction: for a given choice of $\omega(r)$ (and keeping the conservative force fixed) we measure κ_F as a function of δt and r and calculate a distance between κ_F from the DPD simulation and κ_F from the microscopic simulations. We may then use some optimization procedure that does not require explicit calculation of derivatives—e.g., the classic downhill simplex method or Monte Carlo methods—to obtain better estimates for $\omega(r)$ (see, e.g., [45] for a review of different suitable optimization methods).

ACKNOWLEDGMENTS

This work was funded (in part) by the EU integrated project No. FP6-IST-FET PACE, by EMBIO, a European Project in the EU FP6 NEST Initiative, and by the Research Councils of Norway and Sweden. We thank the European Center for Living Technology (ECLT) in Venice, Italy, for providing excellent conditions for a workshop where large parts of the work were mapped out. We also wish to thank the anonymous referees for valuable comments and literature references.

[1] U. Frisch, B. Hasslacher, and Y. Pomeau, Europhys. Lett. **56**, 1505 (1986).
[2] D. C. Rapaport, *The Art of Molecular Dynamics Simulation* (Cambridge University Press, Cambridge, England, 1997).
[3] J. Monaghan, Annu. Rev. Astron. Astrophys. **30**, 543 (1992).
[4] P. J. Hoogerbrugge and J. M. V. A. Koelman, Europhys. Lett. **19**, 155 (1992).
[5] M. Praprotnik, L. D. Site, and K. Kremer, J. Chem. Phys. **123**, 224106 (2005).
[6] M. Praprotnik, L. D. Site, and K. Kremer, J. Chem. Phys. **126**, 134902 (2007).
[7] R. D. Groot and P. B. Warren, J. Chem. Phys. **107**, 4423 (1997).
[8] B. M. Forrest and U. W. Suter, J. Chem. Phys. **102**, 7256 (1995).
[9] R. Henderson, Phys. Lett. **49A**, 197 (1974).
[10] M. S. Green, J. Chem. Phys. **22**, 398 (1954).
[11] R. Kubo, J. Phys. Soc. Jpn. **12**, 570 (1957).
[12] P. Español and P. Warren, Europhys. Lett. **30**, 191 (1995).
[13] P. V. Coveney and P. Español, J. Phys. A **30**, 779 (1997).
[14] C. Marsh, G. Backx, and M. H. Ernst, Europhys. Lett. **38**, 411 (1997).
[15] C. A. Marsh, G. Backx, and M. H. Ernst, Phys. Rev. E **56**, 1676 (1997).
[16] C. A. Marsh and J. M. Yeomans, Europhys. Lett. **37**, 511 (1997).
[17] J. C. Shillcock and R. Lipowsky, J. Chem. Phys. **117**, 5048 (2002).
[18] S. Yamamoto, Y. Maruyama, and S. Hyodo, J. Chem. Phys. **116**, 5842 (2002).
[19] S. Yamamoto and S. Hyodo, J. Chem. Phys. **118**, 7937 (2003).
[20] S. Y. Trofimov, E. L. F. Nies, and M. A. J. Michels, J. Chem. Phys. **117**, 9383 (2002).
[21] N. S. Martys, J. Rheol. **49**, 411 (2004).
[22] E. G. Flekkøy, P. V. Coveney, and G. De Fabritiis, Phys. Rev. E **62**, 2140 (2000).
[23] E. G. Flekkøy and P. V. Coveney, Phys. Rev. Lett. **83**, 1775 (1999).
[24] G. De Fabritiis, P. V. Coveney, and E. G. Flekkøy, Philos. Trans. R. Soc. London, Ser. A **360**, 317 (2002).
[25] P. Español, in *Novel Methods in Soft Matter Simulations*, edited by M. Karttunen, I. Vattulainen, and A. Lukkarinen (Springer, Berlin, 2003), pp. 69–115.
[26] R. Zwanzig, J. Chem. Phys. **33**, 1338 (1960).
[27] R. Zwanzig, *Nonequilibrium Statistical Mechanics* (Oxford University Press, Oxford, 2002).
[28] H. Mori, Prog. Theor. Phys. **33**, 423 (1965).
[29] H. Mori, Phys. Rev. **112**, 1829 (1958).
[30] C. Junghans, M. Praprotnik, and K. Kremer, Soft Matter **4**, 156 (2008).
[31] T. Soddemann, B. Dünweg, and K. Kremer, Phys. Rev. E **68**, 046702 (2003).
[32] M. H. Ernst, E. H. Hauge, and J. M. J. van Leeuwen, Phys. Rev. A **4**, 2055 (1971).
[33] R. Zwanzig and M. Bixon, Phys. Rev. A **2**, 2005 (1970).
[34] P. Español, Phys. Rev. E **52**, 1734 (1995).
[35] A. Lyubartsev, M. Karttunen, I. Vattulainen, and A. Laaksonen, Soft Mater. **1**, 121 (2002).
[36] T. Murtola, E. Falck, M. Patra, M. Karttunen, and I. Vattulainen, J. Chem. Phys. **121**, 9156 (2004).
[37] A. Soper, Chem. Phys. **202**, 295 (1996).
[38] D. Reith, M. Pütz, and F. Müller-Plathe, J. Chem. Phys. **24**,

1624 (2003).
[39] S. Izekov, M. Parrinello, C. J. Burnham, and G. A. Voth, J. Chem. Phys. **120**, 10896 (2004).
[40] N. Almarza and E. Lomba, Phys. Rev. E **68**, 011202 (2003).
[41] A. P. Lyubartsev and A. Laaksonen, Phys. Rev. E **52**, 3730 (1995).
[42] C. Gardiner, *Handbook of Stochastic Methods for Physics, Chemistry, and Natural Sciences*, 3rd ed., Vol. 13 of Springer Series in Synergetics (Springer, Berlin, 2004).
[43] A. D. Gordon, *Classification*, 2nd ed. (Chapman and Hall/CRC, London, 1999).
[44] M. Praprotnik, S. Matysiak, L. D. Site, K. Kremer, and C. Clementi, J. Phys.: Condens. Matter **19**, 292201 (2007).
[45] W. H. Press, S. A. Teukolsky, W. T. Vetterling, and B. P. Flannery, *Numerical Recipes: The art of scientific computing*, 3rd ed. (Cambridge University Press, New York, 2007).